Journal of Membrane Science 668 (2023) 121164

Contents lists available at ScienceDirect

Journal of Membrane Science

journal homepage: www.elsevier.com/locate/memsci

Relating uncharged solute retention of polyelectrolyte multilayer nanofiltration membranes to effective structural properties

Moritz A. Junker [a], Wiebe M. de Vos [a], Joris de Grooth [a,b], Rob G.H. Lammertink [a,*]

[a] Membrane Science and Technology, University of Twente, MESA+ Institute for Nanotechnology, P.O. Box 217, 7500 AE, Enschede, The Netherlands
[b] NX Filtration, Josink Esweg 44, 7545 PN, Enschede, The Netherlands

ARTICLE INFO

Keywords:
Nanofiltration
Polyelectrolyte Multilayers
Transport modeling
Pore size distribution

ABSTRACT

A novel way of making Nanofiltration (NF) membranes is to apply the Layer-by-Layer method, where polyelectrolytes are alternatingly coated on top of a porous Ultrafiltration membrane to form a separation layer with a controllable thickness in the nanometer range, also known as Polyelectrolyte Multilayer (PEM). An important precondition to make use of the variety this fabrication method offers for membrane optimization is knowledge of design rules. Therefore, the structural properties of PEMs and their relation to both coating conditions and membrane performance is an ongoing field of research. In this work, the separation performance of NF PEM membranes, based on PDADMAC/PSS and PAH/PAA, towards uncharged molecules is related to PEM structure. The structure of the membrane is represented by a nanoporous film with distribution in pore size. As, up to date, no experimental technique is available to directly measure pore sizes in the nanometer range of a wet film, a representative pore size distribution is estimated via the use of a theoretical transport description fitted to experimental data. Here, the studied PEM systems showed distinctive differences in both film thickness (PDADMAC/PSS: 44 nm/BL, PAH/PAA: 689 nm/BL) and mean pore size (PDADMAC/PSS: 0.44 nm, PAH/PAA: 0.27 nm). Within the range of layer numbers, the pore size of both PEMs in the layer dominated regime was independent of layer number. This indicates that there is an optimum layer number for PEM NF membranes regarding uncharged solute retention. Surprisingly, despite forming much thicker layers the PAH/PAA system closes off the support membrane pores at a higher bilayer number.

1. Introduction

Nanofiltration (NF) is a pressure-driven membrane process with its main application in the treatment of waste and drinking water [1–3], but also potential application in other fields such as food- [4,5], pharmaceutical- [6] and textile-industry [7]. What makes NF highly competitive in these applications is its unique separation capability at relatively mild conditions and low energy consumption compared to conventional or alternative processes.

Separation in NF is mainly based on the size and charge of solutes [1,2]. With nominal pore sizes in the range of 1 nm, NF membranes are capable to retain neutral solutes with a molecular weight in a range of 100–5000 Da. The rejection of charged solutes is governed by two additional mechanisms. The first, called Donnan Exclusion, is caused by functional groups at the membrane surface that become charged in an aqueous solution. The second, called Dielectric Exclusion, is caused by a difference in dielectric properties between the membrane and solvent phase. As a result of these mechanisms, NF membranes typically have high retention towards multivalent ions and low to moderate retention towards monovalent ions. These separation characteristics are desirable in water purification processes such as water softening [3,8] and removal of organic micropollutants [3,9].

There are, however, certain drawbacks of NF that hinder its widespread application. Amongst these are fouling, limited separation capability and short membrane lifetime [10]. In addition to altering process conditions, membrane characteristics can be adjusted to tackle these challenges. This includes the development of membranes with high chemical and mechanical stability, resulting in a long membrane lifetime and resistance to chemical cleaning. A lot of research is also dedicated to enhancing the separation capability of NF membranes by fine-tuning pore size distribution and charge [11,12].

The market of NF membranes is dominated by Thin Film Composite (TFC) type membranes [13,14]. The TFC design combines the need for membranes to withstand high pressures and allow high water permeation by dividing these functionalities into two layers: a thick layer (order of magnitude 100 μm) with large pores is coated with a thin layer (order of magnitude 100 nm) that has NF properties.

* Corresponding author.
E-mail address: r.g.h.lammertink@utwente.nl (R.G.H. Lammertink).

https://doi.org/10.1016/j.memsci.2022.121164
Received 3 June 2022; Received in revised form 28 October 2022; Accepted 3 November 2022
Available online 9 November 2022

Glossary and Symbols

ΔP_e	Effective transmembrane pressure (Pa)
Δr	Discretization increment of pore size distribution (m)
Δx_e	Effective membrane thickness (m)
η	Viscosity of water (Pas)
λ_i	Ratio of Stokes radius to effective pore radius (–)
ϕ	Ratio of Peclet to Sherwood number under no suction conditions, to determine suction correction (–)
Φ_i	Steric partitioning coefficient (–)
ρ	Density of water (Pas)
σ	Standard deviation in pore size distribution (m)
A_m	Active membrane area (m^2)
B	Salt permeability constant (ms^{-1})
c_b	Solute concentration in the bulk solution ($molm^{-3}$)
c_f	Solute concentration in the feed ($molm^{-3}$)
c_m	Solute concentration at the membrane surface ($molm^{-3}$)
c_p	Solute concentration on permeate side of membrane ($molm^{-3}$)
d	Hollow fiber inner diameter (m)
D_p	Hindered diffusion coefficient inside the pore (m^2s^{-1})
$D_{i,\infty}$	Binary diffusion constant of solute in water (m^2s^{-1})
f	Relative amount of non-selective flux (–)
f_F	Relative impact of pore size on flux (–)
f_N	Relative amount of pores by number (–)
J_w	Permeate flux (ms^{-1})
$J_{w,i}$	Flux through imperfections (ms^{-1})
k	Mass transfer coefficient (ms^{-1})
k^*	Corrected mass transfer coefficient (ms^{-1})
k_B	Boltzmann constant ($m^2kgs^{-2}K^{-1}$)
K_c	Hindrance factor for convective transport (–)
K_d	Hindrance factor for diffusive transport (–)
L	Hollow fiber length (m)
m_p	Permeate mass (m^3)
M_W	Molecular weight (Da)
P_w	Pure water permeability ($ms^{-1}Pa^{-1}$)
Pe_m	Peclet number of membrane transport (–)
R_h	Hydraulic resistance (m^{-1})
r_m	Most abundant pore size (m)
r_p	Effective pore radius (m)
r_s	Stokes radius (m)
r_{max}	Pore size with highest relative flux (m)
Re	Reynolds number (–)
Ret	Observed membrane retention (–)
Ret_{int}	Intrinsic retention (–)
Sc	Schmidt number (–)
Sh	Sherwood number (–)
T	Temperature (K)
t	Time (s)
BL	Bilayer
EtOH	Ethanol
GPC	Gel Permeation Chromatography
HF	Hollow Fiber
LbL	Layer-by-Layer
MSE	Mean Squared Error
MWCO	Molecular Weight Cut-Off
NF	Nanofiltration
PAA	Poly(acrylic acid)
PAH	Poly(allylamine hydrochloride)
PDADMAC	Poly(diallyldimethylammonium chloride)
PEG	Polyethylene glycol
PEM	Polyelectrolyte Multilayer
PES	Polyethersulfone
PSS	Poly(sodium 4-styrenesulfonate)
RO	Reverse Osmosis
TFC	Thin Film Composite
TMP	Transmembrane pressure
UF	Ultrafiltration

The discovery of TFC membranes is deservedly considered a milestone in membrane technology, as it improved membrane performance (originally of RO membranes) considerably [15]. However, there is still room for improvement in the current commercial TFC NF membranes. For instance, does the material of the dense separation layer (typically polyamide) have a low resistance towards chlorine [16], which is present in standard chemicals used for membrane cleaning. Also, the separation performance of these membranes is limited by an upper bound for the trade-off between permeability and selectivity. To overcome this upper bound, multiple characteristics of the separation layer have to be optimized simultaneously [12]. Therefore to make significant advances in NF membranes, new methods with fine control over membrane properties are required.

One promising alternative to fabricate NF membranes is based on Polyelectrolyte Multilayers (PEMs) using the Layer-by-Layer (LbL) method, a concept already introduced almost 20 years ago [17,18]. Here, maintaining the TFC design, a dense polymeric network with NF properties is formed on top of a support membrane by alternatingly coating polyanions and polycations. The main advantage of the LbL method is that the chemistry and structure of the polymeric network can be tuned in a fairly simple and straightforward way by a variety of parameters, such as type of polyelectrolytes, ionic strength and pH of coating solution [19,20]. This way membranes with high chemical and physical stability, advanced separation characteristics and extremely thin separation layers can be fabricated [21]. The high versatility of LbL further allows for functionalization of the membrane surface to reduce membrane fouling for example [22]. The high potential of this novel method resulted in the recent commercialization of hollow fiber (HF) NF membranes based on PEMs.

Compared to established membrane fabrication methods, the LbL method is relatively young. As a result, although there has been a lot of progress in the field, the knowledge on fine-tuning membrane properties for specific applications is far from complete. For this method to reach its full potential, a more complete understanding of the influence of fabrication conditions on PEM structure as well as the influence of PEM structure on membrane performance is required.

One limitation in understanding the mentioned relations is the structural characterization of the PEM based selective layer. As characteristic dimensions are in the nanometer range, the availability of adequate analytical methods is limited. In addition, the significant influence of water on the PEM structure [23,24] requires measurements in a liquid environment. Therefore directly obtaining the internal structural properties of PEMs is challenging. Just to mention a few state-of-the-art characterization techniques that are used to determine

properties of PEMs that are relevant for NF: streaming potential (surface charge) [25], neutron reflectometry (thickness and swelling) [26] and radiolabeling (net charge) [27].

An alternative characterization technique to determine properties relevant to membrane performance, that has been used for conventional polyamide-based NF membranes [28–31], is the indirect determination by relating the filtration performance to an effective structure via the use of transport models. These models can further be used to predict the performance of an NF process.

Clearly, to exploit the full potential of PEM based NF membranes a more elaborate understanding of the interplay between structure and transport processes is required. In this work, we utilize theoretical transport models that account for distribution in effective membrane pore size to describe polyethylene glycol (PEG) transport through two PEM based NF membranes (PDADMAC/PSS and PAH/PAA). The fitted model parameters and their relation to actual structural properties of the PEM are assessed by comparison to supplementary characterization methods as well as previous observations in the literature. This method allows us to gain further understanding of the relationship between structural properties to membrane properties of PEMs and is a step towards rational membrane design.

2. Experimental setup

2.1. Materials

Poly(diallyldimethylammonium chloride) (PDADMAC, M_w 200–350 kDa, 20% in H_2O), poly(sodium 4-styrenesulfonate) (PSS, M_w 200 kDa, 30% in H_2O), poly(acrylic acid) (PAA, M_w 250 kDa, 35% in H_2O), magnesium sulfate heptahydrate (ReagentPlus®, ≥99%), hydrochloric acid (ACS reagent, 37% in H_2O), sodium hydroxide (BioXtra, ≥98%), ethylene glycol (anhydrous 99.8%) and diethylene glycol (ReagentPlus®, 99%) were purchased from Sigma Aldrich. Polyethylene glycol (PEG) with average molecular weights of 200 Da, 600 Da (≥97.4%), 1000 Da (≥97.8%), 2000 Da (≥97.8%) and 3000 Da (≥98.8%), as well as glycerol (EMSURE®Reag. Ph Eur, 85%) were purchased from Merck. Poly(allylamine hydrochloride) (PAH, M_w 150 kDa, 40% in H_2O) was purchased from Nittobo. Polyethylene glycol with an average molecular weight of 400 Da was purchased from Alpha Aesar. Ethanol (100%) was purchased from Boom B.V. (Netherlands). Sodium chloride (>99.96%) was kindly provided by AkzoNobel. All chemicals were used without further purification. Hollow fiber (HF) ultrafiltration (UF) membranes made of modified polyethersulfone (PES) were kindly provided by NX Filtration B.V. (Enschede, the Netherlands). For all H_2O solutions, MiliQ water with a resistance of at least 18.2 MΩcm was used.

2.2. Membrane fabrication

Before dip coating, the HF UF support membranes (MWCO ~10 kDa, Permeability ~150 LMHbar, inner diameter 0.7 mm, negative charge) were immersed in 10% EtOH solution in H_2O followed by rinsing in H_2O, to remove added compounds for dry storage. The rinsed fibers were subsequently dip coated using the Layer-by-Layer (LbL) method to build polyelectrolyte multilayers on top of the support. In the first step of this method, the fibers are immersed in the polycation solution (0.1 gL^{-1}, 50 mM NaCl, pH 5.5) for 15 min. In the next step, which is repeated three times, the fibers are rinsed in 50 mM NaCl solution for 5 min, to wash off any residual polycation solution. The following steps include the immersion in a polyanion solution (0.1 gL^{-1}, 50 mM NaCl, pH 5.5) for 15 min, again, followed by three times rinsing in 50 mM NaCl solution for 5 min. This sequence completes one bilayer (BL). Here, two polyelectrolyte systems PDADMAC/PSS (up to 10 BL) and PAH/PAA (up to 14 BL) were studied. The pH value of the coating solutions was adjusted with 1 M NaOH/HCl solutions. After the LbL procedure, the membranes were immersed in a 15% glycerol in H_2O solution for at least 4 h before drying.

2.3. Membrane performance evaluation

To evaluate the performance of the fabricated membranes, single fiber modules with an active fiber length of about L=18 cm (active membrane area of A_m=3.95 cm^2) were prepared in quadruplicate. Using a crossflow filtration setup (see Supporting Information S1), previously described in [32], 16 membrane modules are tested simultaneously. The temperature of the feed solution is regulated at 20 ± 1 °C. The crossflow velocity within the fibers is set to 1 ± 0.05 ms^{-1} to limit the extent of concentration polarization. After rinsing the modules with H_2O to remove any residual glycerol, the pure water permeability is measured at constant transmembrane pressures (TMP) of 2, 3 and 4 bar (estimated variation ±0.05 bar). The pure water permeability P_w ($Lm^{-2}h^{-1}bar^{-1}$) can be calculated using the following equation:

$$P_w = \frac{m_p}{\rho_w \cdot A_m \cdot t \cdot TMP} \tag{1}$$

where m_p (g) is the permeate mass collected within the time t (h), ρ_w (998.21 gL^{-1}) is the density of water at 20 °C, A_m (m^2) is the active membrane area and TMP (bar) the applied transmembrane pressure. Using Darcy's law, the pure water permeability can be alternatively displayed as the hydraulic resistance R_h (m^{-1}):

$$R_h = \frac{1}{\eta \cdot P_w} \tag{2}$$

where η (1.0016 $\cdot 10^{-3}$ Pas) is the viscosity of water at 20 °C and P_w (now expressed in $ms^{-1}Pa^{-1}$) the pure water permeability. The $MgSO_4$ retention (feed concentration of 5 mM) was measured at a constant TMP of 3 bar and 5 bar for the PDADMAC/PSS and PAH/PAA membranes, respectively. The PEG retention (1 gL^{-1}) was measured at three different TMP values (PDADMAC/PSS: 1, 2, 3 bar; PAH/PAA: 2, 3.5, 5 bar) for each membrane. The retention Ret (-) is defined as:

$$Ret = 1 - \frac{c_p}{c_f} \tag{3}$$

where c_p ($molL^{-1}$) and c_f ($molL^{-1}$) are the solute concentration in the permeate and feed, respectively.

2.4. Analytical methods

$MgSO_4$ concentrations were determined via conductivity measurements using a portable conductivity meter (Cond^{TM} 3210, WTW^{TM} GmbH). PEG concentrations were determined via Gel Permeation Chromatography (GPC). The GPC setup (Agilent 1200/1260 Infinity GPC/SEC series) uses two columns (Suprema 8 × 300 mm, 1000 Å–30 Å, 10 μm, Polymer Standards Service GmbH) in series and a refractive index detector (Agilent 1100 HPLC G1362 A RID Detector). The flow rate of the eluent (50 mgL^{-1} NaN_3 in H_2O) is 1 $mLmin^{-1}$. Information on the deconvolution method of the detector signal is given in the Supporting Information S2.

3. Theoretical transport model

3.1. Salt retention

To transform the retention of $MgSO_4$ (a process parameter) into the salt permeability B (ms^{-1}) (an intrinsic membrane parameter) the film model with a mass transfer correlation is applied, as described in [33]:

$$B = \left(\frac{1 - Ret}{Ret}\right) \cdot \left(J_w - \frac{J_w^2}{k^*}\right) \tag{4}$$

Here J_w (ms^{-1}) is the permeate flux and k^* (ms^{-1}) is the mass transfer coefficient corrected for suction, which is determined via [34,35]:

$$\overline{Sh} = \frac{kd}{D_s} = 1.62\left(ReSc\frac{d}{L}\right)^{\frac{1}{3}} - 1.2 - 0.28\left(ReSc\frac{d}{L}\right)^{-\frac{1}{3}} \tag{5}$$

$$\frac{k^*}{k} = \phi + (1 + 0.26\phi^{1.4})^{-1.7} \tag{6}$$

Here, Sh (-) is the dimensionless Sherwood number, k (ms^{-1}) is the mass transfer coefficient at no flux, d (m) is the HF inner diameter, D_s ($0.75 \cdot 10^{-9}$ m^2s^{-1} [36]) is the diffusion coefficient of $MgSO_4$ at 20 °C, $Re = \rho d v/\eta$ (-) is the dimensionless Reynolds number, $Sc = \eta/(\rho D_s)$ (-) is the dimensionless Schmidt number, L (m) the HF length and $\phi = J_w/k$ the ratio of flux J_w (ms^{-1}) to mass transfer coefficient at no flux k (ms^{-1}). The applied mass transfer correlation is valid for the laminar flow regime (Re<2300) and low recovery values. For high recovery values an additional correction factor should be applied [33]. For very small Reynolds numbers (Re<0.16) Eq. (5) gets negative. Operation conditions of hollow fiber membranes, however, do not approach this limit.

3.2. PEG retention

To transform the retention of the PEG mix, which is again a process parameter, to an intrinsic membrane property, we apply a simplified version of the well known Donnan Steric Pore Model and Dielectric Exclusion (DSPM&DE) model [37,38]. Here, we represent the membrane by a bundle of straight cylindrical pores. Although the actual membrane (or PEM) structure is likely far from this commonly applied idealized geometry [29,30,37–40], this simplified theoretical description serves the purpose of this work well, which is to describe membrane transport, monitor selective layer build-up and qualitatively compare different PEM systems. As the PEG solutes are uncharged in solution, the exclusion mechanism of the DSPM&DE model reduces to steric exclusion, while the transport within the pores is described by advection and diffusion. To model the retention of PEG molecules based on steric exclusion, one needs to approximate their size in solution. Here we choose to use the hydrodynamic radius $r_{i,s}$ (m) based on Stokes–Einstein equation [41]:

$$r_{i,s} = \frac{k_B T}{6\pi\eta D_{i,\infty}} \tag{7}$$

with the Boltzmann constant k_B ($1.381 \cdot 10^{-23}$ $m^2kgs^{-2}K^{-1}$) and the solution temperature T (293.15 K). Here, $D_{i,\infty}$ (m^2s^{-1}) is the solute diffusion coefficient in infinite dilution which is approximated using a correlation [42] (corrected for temperature and viscosity):

$$D_{i,\infty} = 1.25 \cdot 10^{-8} M_w^{-0.55} \cdot \frac{293.15\,\mathrm{K}}{298.15\,\mathrm{K}} \frac{0.89 \cdot 10^{-3}\ \mathrm{Pas}}{1.0016 \cdot 10^{-3}\ \mathrm{Pas}} \tag{8}$$

with M_w (Da) being the molecular weight of the PEG molecule. As we did not find a range of molecular weights of PEG for which this formula is valid, we compared it to literature data of diffusion coefficient measurements in the range of interest. A graph comparing the correlation to measurement values can be found in the Supporting Information S3. For the relevant range of this study (MW ≤ 3000 Da) the correlation fits reasonably well. Also shown is the alternative correlation used to estimate the influence of error in PEG diffusion coefficient.

3.2.1. Single pore size

In the standard form, the DSPM&DE model assumes uniform pores with a singular effective pore radius, to describe the steric exclusion. Therefore, the membrane is represented by two parameters: the effective membrane thickness Δx_e (m) (which combines pore length, tortuosity and porosity) and the effective pore radius r_p (m). These can be determined by fitting the model to pure water permeability and uncharged solute retention. Details on the fitting procedure can be found in the Supporting Information S4. The system of equations describing the membrane transport after simplifications reduces to:

$$J_w = \frac{r_p^2}{8\eta\Delta x_e}\Delta P_e \tag{9}$$

$$Ret_{int} = 1 - \frac{K_{i,c}\Phi_i}{(K_{i,c}\Phi_i - 1)\cdot \exp(-Pe_m) + 1} \tag{10}$$

$$Pe_m = \frac{K_{i,c} J_w \Delta x_e}{D_{i,p}} \tag{11}$$

$$\Phi_i = (1 - \lambda_i)^2 \tag{12}$$

$$D_{i,p} = K_{i,d} D_{i,\infty} \tag{13}$$

$$\lambda_i \le 0.95 : K_{i,d} = \frac{\begin{bmatrix} 1 + (9/8)\lambda_i \ln\lambda_i - 1.56034\lambda_i \\ +0.528155\lambda_i^2 + 1.91521\lambda_i^3 - 2.81903\lambda_i^4 \\ +0.270788\lambda_i^5 + 1.10115\lambda_i^6 - 0.435933\lambda_i^7 \end{bmatrix}}{(1-\lambda_i)^2} \tag{14}$$

$$\lambda_i > 0.95 : K_{i,d} = 0.984\left(\frac{1-\lambda_i}{\lambda_i}\right)^{\frac{5}{2}} \tag{15}$$

$$K_{i,c} = \frac{1 + 3.867\lambda_i - 1.907\lambda_i^2 - 0.834\lambda_i^3}{1 + 1.867\lambda_i - 0.741\lambda_i^2} \tag{16}$$

$$Ret = 1 - \frac{(1 - Ret_{int})k_i^*}{k_i^* - Ret_{int} J_w} \tag{17}$$

J_w (ms^{-1}) is the permeate flux, η ($1.0016 \cdot 10^{-3}$ Pas) is the viscosity of water at 20 °C, ΔP_e (Pa) is the effective transmembrane pressure accounting for osmotic pressure (in the case of pure water measurements ΔP_e=TMP), Ret_{int} (-) is the intrinsic membrane retention (in the ideal case of no concentration polarization), Ret (-) is the observed retention (as defined in Eq. (3)), Pe_m (-) is the Peclet number of transport through the membrane, k_i^* (ms^{-1}) is the corrected mass transfer coefficient (determined as described in Eq. (5) and (6)), Φ_i (-) is the steric partitioning coefficient, λ_i (-) is the ratio of solute Stokes radius to effective pore radius ($\lambda_i = r_{i,s}/r_p$), $D_{i,p}$ (m^2s^{-1}) is the hindered diffusion within the nanopore, $K_{i,c}$ (-) the hindrance factor for convective transport, $D_{i,\infty}$ (m^2s^{-1}) the solute diffusion coefficient in infinite dilution, and $K_{i,d}$ (-) the hindrance factor for diffusive transport.

3.2.2. Pore size distribution

To extend the model from a single pore radius to a pore size distribution, we introduce a discrete log-normal distribution function to describe the relative abundance of a range of pore sizes, in a similar way as it was presented by [28]. The continuous log-normal distribution is describe by:

$$f_N(r_p) = \frac{1}{r_p\sqrt{2\pi b}} \exp\left(-\frac{(\ln\frac{r_p}{r_m} + \frac{b}{2})^2}{2b}\right) \tag{18}$$

$$b = \ln\left(1 + \left(\frac{\sigma}{r_m}\right)^2\right) \tag{19}$$

where f_N (-) is the relative amount by number of pores, r_p (m) the pore size, r_m (m) the mean pore size and σ (m) is the standard deviation in pore size distribution. To allow for numerical solution, this equation has to be discretized by integrating over a range of pore size:

$$f_{N,d}(r_p) = \int_{r_p - \frac{\Delta r}{2}}^{r_p + \frac{\Delta r}{2}} f_N(r)\,dr \tag{20}$$

Here $f_{N,d}$ (-) is the discretized distribution of relative number and Δr (0.01 nm) is the discretization step size (determined from a mesh refinement study shown in the Supporting Information S5). In addition, the pore size distribution function is truncated, which has been shown to increase fit quality [28], and reduces computation time. For the truncation, as well as for fitting, the distribution is transformed to a distribution based on relative flux $f_{F,d}$ (-):

$$f_{F,d}(r_p) = \frac{f_{N,d}(r_p) r_p^4}{\sum_{r_p=r_{min}}^{r_{max}} f_{N,d}(r_p) r_p^4} \tag{21}$$

The truncation is made at a value of 5% of the maximum value of $f_{F,d}$. After that, the distribution is normalized to assure that the sum over $f_{F,d}$ equals 1. To calculate the retention, we calculate the retention and flux for each pore size and calculate the overall retention Ret (-) via:

$$Ret = \frac{\sum_{r_p=r_{min}}^{r_{max}} J_{w,r}(r_p) Ret_r(r_p)}{J_w} \tag{22}$$

with $J_{w,r}$ (ms^{-1}) the permeate flux through a discrete pore radius and Ret_r (-) the retention by a discrete pore radius. For each discrete pore radius, the single pore size model can be applied, where the effective membrane thickness has to be updated according to:

$$\Delta x_{e,d} = \frac{\sum_{r_p=r_{min}}^{r_{max}} \pi r_p^4 f_{N,d}(r_p)}{8\eta P_w} \tag{23}$$

$\Delta x_{e,d}$ (m^3) is the effective membrane thickness updated for the pore size distribution and P_w ($ms^{-1}Pa^{-1}$) the pure water permeability. The permeate flux through a discrete pore radius $J_{w,r}$ is calculated via:

$$J_{w,r} = \frac{\pi r_p^4 f_{N,d}}{8\eta \Delta x_{e,d}} \Delta P_e \tag{24}$$

The parameter $\Delta x_{e,d}$ accounts for fractions of the different pore sizes to the overall flux and cannot be directly compared to measured thickness values. To estimate the real thickness of the membrane and also compare it to single pore size results, the effective thickness $\Delta x_{e,d}$ for the pore size distribution was again transformed using the pore radius with maximum contribution to the relative flux:

$$\Delta x_e = \frac{r_{max}^2}{8\eta P_w} \tag{25}$$

3.2.3. Imperfections

To account for the presence of imperfections causing leakage of feed solution, e.g. module related leakage or pinholes, we assume an additional non-selective flux in parallel to the PEM:

$$J_w = J_{w,m} + J_{w,i} \tag{26}$$

Here, the permeate flux J_w (ms^{-1}) is composed of the permeate flux through the active separation layer $J_{w,m}$ (ms^{-1}) and the non-selective flux through imperfections $J_{w,i}$ (ms^{-1}). The relative amount of non-selective flux f (%) of the complete permeate flux is introduced:

$$f = \frac{J_{w,i}}{J_w} \cdot 100\% \tag{27}$$

The observed retention of the membrane module can then simply be calculated via:

$$Ret = 1 - \frac{c_{p,s}(1-f) + c_m f}{c_b} \tag{28}$$

Here, $c_{p,s}$ ($molm^{-3}$) is the permeate concentration of the selective layer and c_m ($molm^{-3}$) is the feed concentration for the non-selective flux.

$$J_w c_{p,s} = -k^*(c_m - c_b) + J_w c_m \tag{29}$$

The concentration c_m at the membrane surface is derived from the film model (Eqs. (5), (6) and (29)) assuming only selective transport.

4. Results and discussion

In the first part of this section (4.1 and 4.2) we present experimental results of the conducted filtration measurements and discuss layer number dependent membrane properties. In the second part of this section (4.3–4.6) we focus on the different theoretical membrane transport models considered in this work and analyze the implied intrinsic PEM properties. In the third part of this section (4.7) we summarize and discuss the structural properties of the two PE systems considering experimental observations of this study as well as previous observations in the literature.

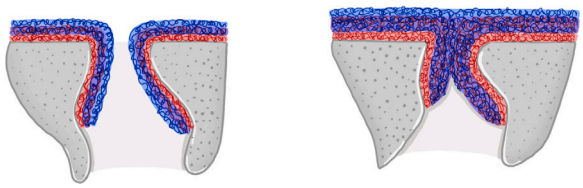

Fig. 1. Illustration of "pore dominated" and "layer dominated" regime in LbL coating of UF membranes to fabricate NF membranes.
Source: Adapted from de Grooth et al. [43].

4.1. Selective layer build-up

To monitor the growth of the PEM layer on top of the UF support, fibers were taken out during the LbL coating procedure for each BL until the final layer was reached. As it has been shown by de Grooth et al. [43], there are typically two regimes observed when coating porous UF support membranes with PEM layers to reach a membrane with NF properties (illustrated in Fig. 1). In the "pore dominated regime", the initial layers do not fully cover the pores of the support membrane, yet. After fully closing the pores of the support, the PEM layer dominates the transport through the membrane ("layer dominated regime"). It is essential to reach the "layer dominated regime" when fabricating PEM based NF membranes. In this regime, the observed filtration performance can directly be related to the intrinsic properties of the PEM. For fabrication purposes (also on a commercial scale) assuring full closure of support pores also increases the reproducibility of membrane properties. Last but not least, the selectivity increases significantly once the pores of the support are fully closed, which is required for NF applications.

One membrane characteristic that indicates pore closing is the pure water permeability. Fig. 2 displays the pure water permeability of the membrane as a function of the BL number for both PEM systems. Also shown is the hydraulic resistance, which is inversely proportional to the pure water permeability (Eq. (2)). For both systems, the pure water permeability decreases with an increasing number of BLs. Moreover, a decrease in the slope of permeability with BL number is observed and the permeability seems to slowly go towards a plateau value. However, one can observe that at high BL numbers the resistance of the PEM systems still increases with layer number. This we attribute to the "layer dominated regime" in which, when considering linear multilayer growth [27,44,45], the layer thickness should increase linearly with layer number and therefore so does the hydraulic resistance. The initial steep decrease in permeability is partially caused by the high sensitivity of permeability to effective membrane thickness ($A \propto \Delta x_e^{-1}$). In the case of PDADMAC/PSS, the increase in hydraulic resistance with BL number decreases after 4 BLs. This indicates the transition between two different layer growth regimes of the PEM NF membrane, where the increase of hydraulic resistance is higher during pore closing and lower but linear for the layer dominated regime. For PAH/PAA, the increase of hydraulic resistance with BL number does not reduce at a distinct BL number in the observed range, so no clear transition can be determined. It even increases slightly after 9 BLs, which will be discussed later. One other option to monitor pore closing that should be mentioned here, which was also shown in [43], is to use the influence of the ending layer ("odd–even effect") on the swelling behavior of the PEM. This is caused by the great influence that the ending layer of a PEM can have on the overall multilayer properties [24,46]. The difference in swelling of positive and negative ending PEMs has exactly opposite effects on pure water permeability in the "pore dominated" and "layer dominated" regimes. Since the transition between the two regimes is not the main focus of this work, but rather the properties of the PEM layer itself, we chose to only consider even BL numbers (negative ending layer). Membranes with a negative surface charge are

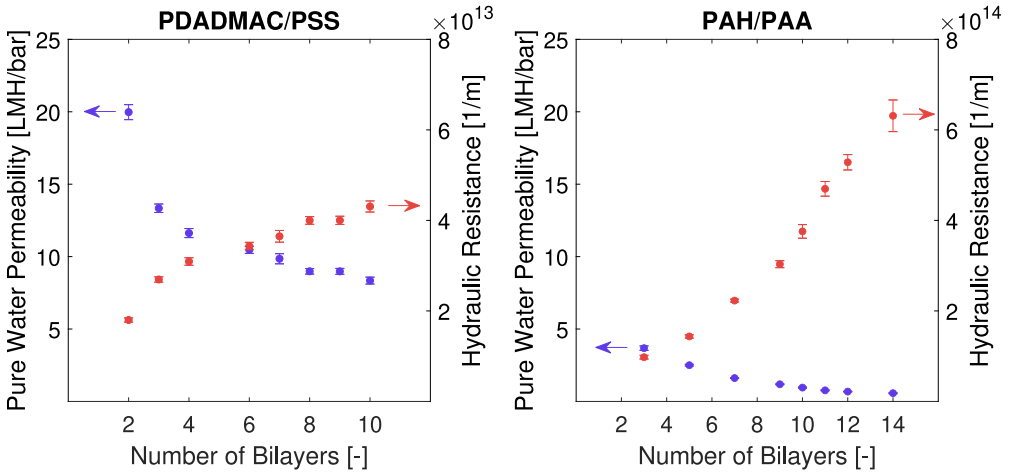

Fig. 2. Pure water permeability [LMH/bar] (left *y*-axis, blue) and hydraulic resistance [1/m] (right *y*-axis, red) as a function of bilayer number. Two Polyelectrolyte Multilayer systems: PDADMAC/PSS (left) and PAH/PAA (right). Mind the scale for the hydraulic resistance. Error bars display the 95% confidence intervals. (For interpretation of the references to color in this figure legend, the reader is referred to the web version of this article.)

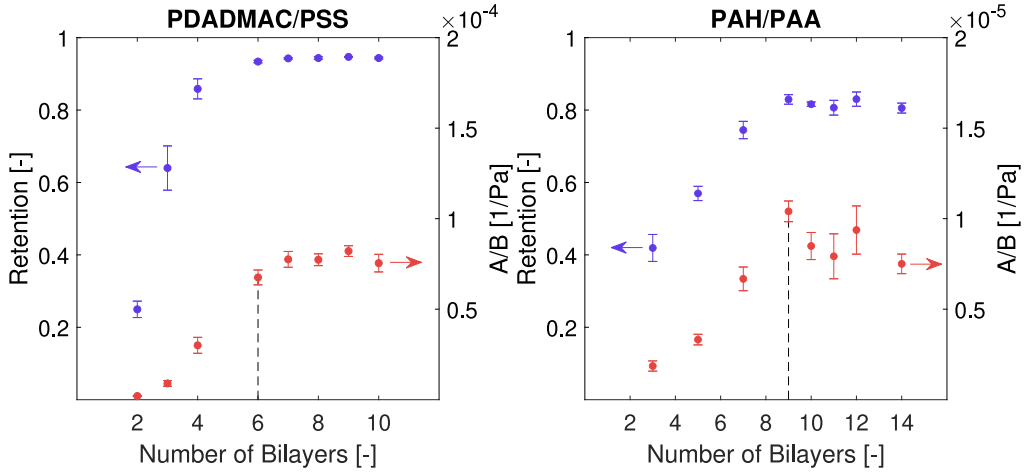

Fig. 3. $MgSO_4$ Retention [-] (left *y*-axis, blue) and A/B [1/Pa] (right *y*-axis, red) as a function of bilayer number. Two Polyelectrolyte Multilayer systems: PDADMAC/PSS (left) and PAH/PAA (right). Mind the scale for A/B. Error bars display the 95% confidence intervals. (For interpretation of the references to color in this figure legend, the reader is referred to the web version of this article.)

typically favored in water treatment, due to their advantageous fouling properties [47–51].

When comparing the two PEM systems, two important differences stand out. First, PAH/PAA based membranes have a significantly higher hydraulic resistance than PDADMAC/PSS based membranes (one order of magnitude). Second, the change in slope of hydraulic resistance over BL number, which we attribute to the closing of the support membrane pores, only appears for the PDADMAC/PSS system at around 4–6 BLs.

One additional characterization method often used to quantify membrane performance is the $MgSO_4$ retention, which is displayed in Fig. 3 as a function of the PEM BL number. For both PEM systems an increase in $MgSO_4$ retention within the first few BLs is observed, which stagnates rather abruptly after a certain BL number. The initial sharp increase in $MgSO_4$ retention, especially for PDADMAC/PSS, is related to the pore closing of the support membrane, which by itself has a very low $MgSO_4$ retention. To translate the observed retention to an intrinsic membrane property, that in addition accounts for water permeability, we fitted the $MgSO_4$ retention to a simple solution–diffusion transport model, while accounting for the effect of concentration polarization. The effective selectivity of water over salt is hereby represented by the ratio of the pure water permeability A over the salt permeability B. We hypothesize, that A/B behaves differently within the two regimes of coating porous support membranes. In the "pore dominated" regime, the reduction in salt permeability B due to surface exclusion and hindered transport within the membrane leads to an increase in selectivity A/B. Although, pure water permeability A experiences a similar decrease in this regime (see Fig. 2), the decrease in salt permeability B is dominating. In the "layer dominated" regime, there is a constant increase in layer thickness with BL number. If one assumes thickness independent intrinsic properties of the PEM film according to the solution–diffusion model, the selectivity A/B should stay constant as both A and B are proportional to the inverse of layer thickness [52]. As shown in Fig. 3, the A/B value as a function of the BL number behaves as predicted for both PEM systems: in the initial layers there is an increase of A/B and after a certain BL number the A/B value stagnates within the range of the 95% confidence intervals. Here, the point of full pore closure is determined at 6 BL and 9 BL for the PDADMAC/PSS and PAH/PAA systems, respectively. Ion transport through PEM NF membranes is governed by both electrostatic and steric interactions. Thus, ion retention measurements alone do not suffice to unambiguously identify the extent of both effects (here it is reasonable to describe solute transport by using a permeability B).

4.2. PEG retention

To isolate the size based hindrance and exclusion mechanisms of the membrane, which can further be related to the structural properties

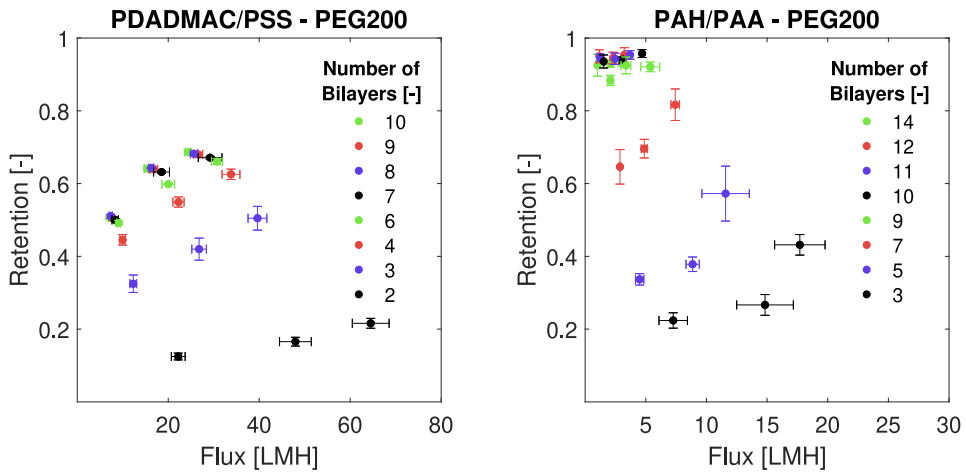

Fig. 4. PEG200 retention [-] as a function of flux [LMH] with increasing number of bilayers [-]. Two Polyelectrolyte Multilayer systems: PDADMAC/PSS (left) and PAH/PAA (right). Error bars display the 95% confidence intervals.

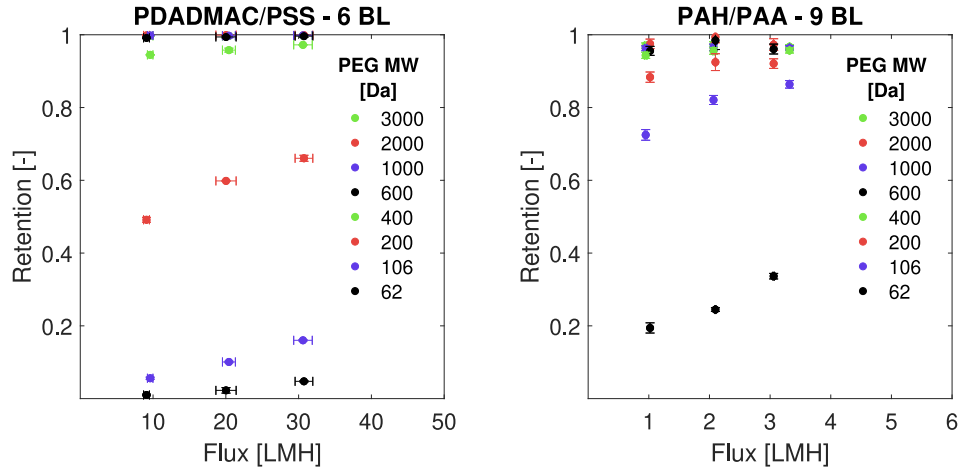

Fig. 5. PEG retention [-] as a function of flux [LMH] with increasing PEG M_w [Da]. Two Polyelectrolyte Multilayer systems: PDADMAC/PSS 6 BLs (left) and PAH/PAA 9 BLs (right). Error bars display the 95% confidence intervals.

of the PEM, we measured the filtration performance for PEG solutions with a range of molecular weights at three different TMPs. For reasons of clarity, in the following, we only show a selected set of results that suffices to demonstrate the qualitatively observed behavior of neutral solute retention. An overview of the observed retention for the full set of measured PEG can be found in the Supporting Information S6.

The dependency of PEG retention on BL number is illustrated in Fig. 4 by means of the PEG 200 Da retention. For a fixed BL number, it is evident that the observed retention increases with permeate flux. This dependency of retention on permeate flux is typical for dense membranes (RO and NF) with significant solute transport via diffusion [33]. The PEG retention as a function of BL number also indicates the two regimes of PEM membrane fabrication. In the "pore dominated" regime, both flux and uncharged solute retention change strongly with BL number. Due to an increase in hydraulic resistance, as already seen in Fig. 2, the permeate flux decreases. At the same time, the closing of the support membrane pores leads to increased steric exclusion of solutes and by that higher observed retention. When reaching the "layer dominated" regime the retention of PEG stagnates and the flux slightly decreases with BL number. From observed PEG retention measurements, however, it is difficult to pinpoint the transition to the "layer dominated" regime.

To compare the two PEM systems directly and independent of support membrane properties, we examine the PEG retention in the "layer dominated" regime, here displayed in Fig. 5. The significant difference in hydraulic resistance leads to lower permeate fluxes for the PAH/PAA compared to the PDADMAC/PSS system (one order of magnitude). At the same time, it can be seen that the retention of PEG ranging from EG to PEG 200 Da is much higher for the PAH/PAA system. These observations suggest a denser structure, here related to mesh/pore size, of PAH/PAA compared to PDADMAC/PSS PEMs coated under these conditions. Both systems reach close to full retention of PEG starting from a molecular weight of 400 Da. This indicates a MWCO below 400 Da for both systems (with $MWCO_{PAH/PAA} < MWCO_{PDADMAC/PSS}$). Lastly, it can also be noticed that the retention of PEGs with molecular weight higher than 600 Da do not reach full retention for the PAH/PAA system, which could be falsely interpreted as imperfections of the PEM system. As will be shown later, the amount of imperfections (in the "layer dominated" regime) for both PEM systems is very similar and does likely result from leakage related to the membrane module preparation. The effect of imperfections in the PAH/PAA modules is however amplified due to the much lower permeability.

The experimentally observed retention of PEG, similar to the $MgSO_4$ retention, is a filtration process parameter. This means, that there are several factors that in addition to the intrinsic membrane properties influence the measured retention. Among these, as already seen, are permeate flux and solute size. One way to allow direct comparison would be to keep all process parameters identical for both PEM systems. Alternatively, one can reduce the retention observed at multiple fluxes and solute sizes to an intrinsic membrane property by means of a

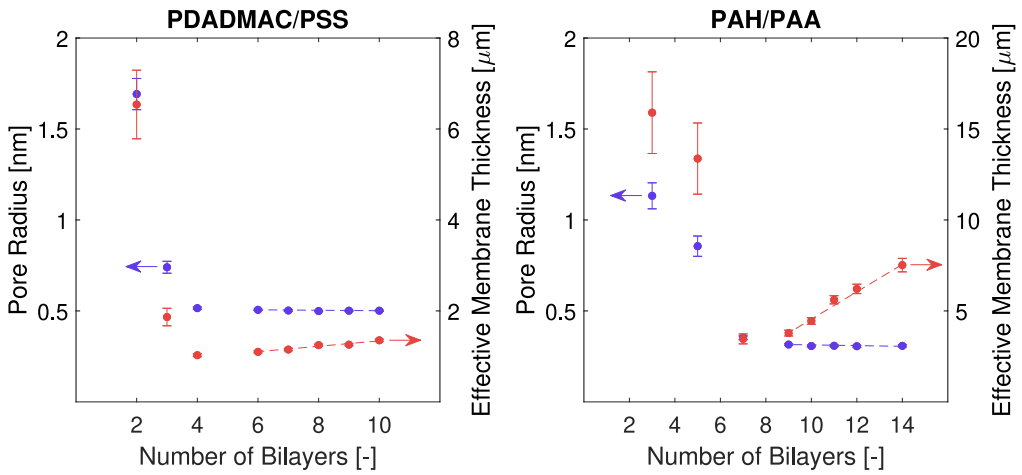

Fig. 6. Fitted effective pore radius [nm] (left *y*-axis, blue) and effective membrane thickness [μm] (right *y*-axis, red) as a function of bilayer number [-]. Two Polyelectrolyte Multilayer systems: PDADMAC/PSS (left) and PAH/PAA (right). Dashed line highlights "layer dominated" regime. Error bars display the 95% confidence intervals. (For interpretation of the references to color in this figure legend, the reader is referred to the web version of this article.)

transport model. There are several potential benefits in the introduction of an intrinsic film property: the model can be applied to predict the retention of uncharged molecules with similar solute-membrane interactions as PEG within the range of process conditions considered (decreasing accuracy for extrapolation), the intrinsic property simplifies direct comparison of PEMs (or other separation films) and the intrinsic property can be directly translated to structural properties of the PEM being studied. Therefore, we fitted the observed retention of PEGs simultaneously at all permeate fluxes and solute sizes for each BL and PEM system using a pore model. The results using different intrinsic membrane properties will be shown in the following sections.

4.3. Effective pore radius

The first, most basic, theoretical representation of the membrane structure assumes parallel cylindrical pores with identical sizes (length and radius). This results in a set of two fitting parameters: effective pore radius and effective membrane thickness. Here, the term "effective" is not only used to emphasize the theoretical nature of these quantities (due to the breakdown of continuum theory below 1 nm [53], these quantities at most indicate the order of magnitude and allow qualitative comparison), but also since the effective membrane thickness is a combination of pore length, membrane porosity and membrane tortuosity.

Fitting the model to the PEG retention measurements and pure water permeability results in an effective pore radius and thickness for each membrane, which is displayed in Fig. 6. To check for the potential influence of PEG on the membrane properties we compare the permeability in both measurements. We find no significant variation in permeability for 10 BLs of PDADMAC/PSS (pure water permeability of $8.3 \pm 0.2\,\mathrm{LMHbar^{-1}}$, permeability during PEG filtration corrected for osmotic pressure during PEG filtration $8.4 \pm 0.1\,\mathrm{LMHbar^{-1}}$) and for 14 BLs of PAH/PAA (pure water permeability of $0.57 \pm 0.03\,\mathrm{LMHbar^{-1}}$, permeability during PEG filtration corrected for osmotic pressure during PEG filtration $0.58 \pm 0.05\,\mathrm{LMHbar^{-1}}$). The dashed lines in the figure highlight the "layer dominated" regime as determined in the previous sections. From the effective pore radius, it can be seen, that in the initial BL the closing of the pores leads to a sharp decrease in pore radius (here the pore radius of the support membrane with a MWCO of 10 kDa is estimated to be around 2–3 nm). Once, the BL number reaches the point of transition to the "layer dominated" regime the effective pore radius becomes constant. The effective membrane thickness does follow a similar trend in the "pore dominated" regime. The reduction in effective thickness during pore closing correlates well to the PEM layer becoming the active separation layer (which is thinner than the active separation layer of the support membrane). Once the "layer dominated" regime is reached, there is a steady increase in effective membrane thickness for both PEM systems. An increase in effective thickness with BL number is expected from a continuous increase in hydraulic resistance, also observed in other studies [21,25,43,54]. One thing to point out, is the higher uncertainty for fitting parameters in the pore dominated regime. We attribute this to both the higher absolute uncertainty at higher permeate fluxes and the high sensitivity of membrane properties to small variations in PEM properties in the region of pore closing. Comparing the two intrinsic membrane properties of the two PEM systems in the "layer dominated" regime, two differences that have been indicated in the experimental results become very apparent. First, the effective pore radius, and with that, the mesh size of the PE network of the PAH/PAA system (0.31 nm) is smaller than the one of the PDADMAC/PSS system (0.5 nm). Secondly, the effective membrane thickness, which is proportional to the actual film thickness and the inverse of porosity, is higher and has a steeper increase for the PAH/PAA system. This indicates that the PAH/PAA network has a higher incremental thickness per BL. In order to improve the prediction capability of the transport model and at the same time the (effective) physical representation of the PEM layer, the model is extended to account for distribution in pore radius.

4.4. Pore size distribution

For commercial TFC NF membranes often a pore size distribution (following a log-normal distribution) is applied to model the transport of uncharged molecules [28–31]. These types of distributions have also been determined experimentally for the surface pores using atomic force microscopy [28,30,55,56]. It is reasonable to assume that the porous network of a PEM can be described by a similar distribution in mesh size. It is known that the internal structure does not consist of fully separated alternating layers, but rather strongly interpenetrating and less ordered layers [23,26,57–61]. Extrinsic charge compensation by ions interrupts the dense network of ionic crosslinks likely causing a larger mesh size with a more heterogeneous distribution [23,43,59]. The ionic network is by itself also more dynamic than covalently crosslinked networks and thereby allows for (small) structural changes over time. Using NMR cryoporometry, Chávez et al. [62] observed a distribution in pore size within a PEM layer. Therefore, we extend the theoretical pore model to account for a log-normal distribution in pore radius.

The resulting best fits of the pore size distribution for a selected set of 6 different BL numbers for both PEM systems are shown in

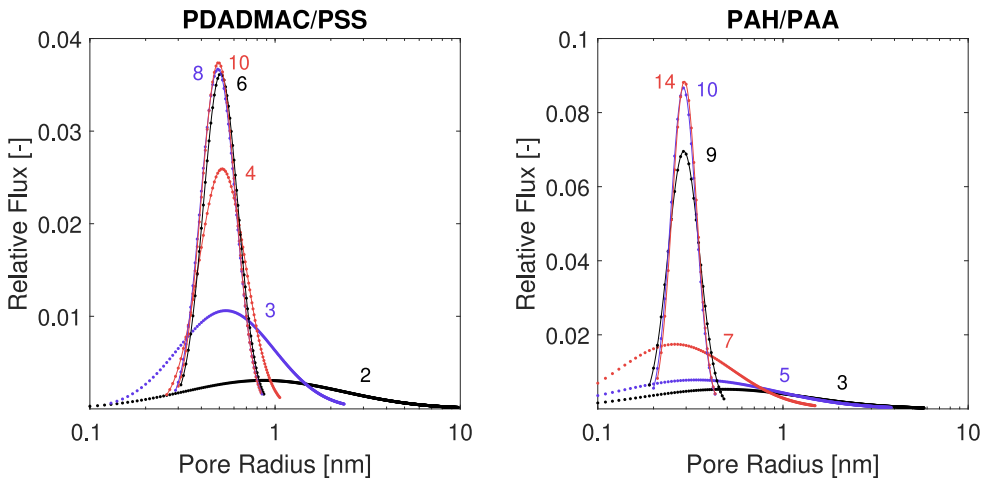

Fig. 7. Log-normal pore size distribution fit. Relative flux [-] as a function of pore radius [nm]. Two Polyelectrolyte Multilayer systems: PDADMAC/PSS (left) and PAH/PAA (right). Discretization size of 0.01 nm. Discrete pore size distributions fitted using a spline function to guide the eye.

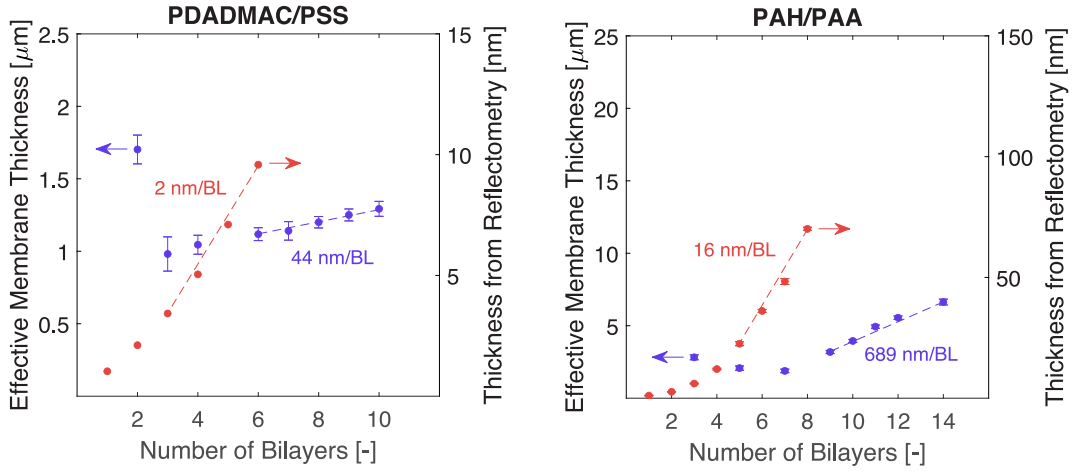

Fig. 8. Log-normal pore size distribution fit. Effective thickness [μm] (left *y*-axis, blue) and thickness measured with Reflectometry [nm] (right *y*-axis, red) as a function of bilayer number [-]. Reflectometry data from [43,54]. Two Polyelectrolyte Multilayer systems: PDADMAC/PSS (left) and PAH/PAA (right). Error bars display the 95% confidence intervals. (For interpretation of the references to color in this figure legend, the reader is referred to the web version of this article.)

Fig. 7. In both systems, similar behavior in the variation of pore size distribution during layer growth can be observed. At low BL numbers ("pore dominated" regime), the membrane is represented by a quite broad distribution in pore size. This can be explained by the only partially closed pores of the support UF membrane with an estimated pore radius in the range of 2–3 nm. With increasing BL numbers, the pore size distribution narrows and shifts to a lower mean pore radius. Both PEM systems progress towards a constant mean pore radius of 0.44 nm and 0.27 nm (corresponding to the highest relative flux at pore radii of 0.49 nm and 0.29 nm) for the PDADMAC/PSS and PAH/PAA system, respectively. As one would expect for narrow distributions such as these, the obtained mean pore sizes in the "layer dominated" regime correspond well with the ones obtained from fitting an average pore radius. The decrease in the mean pore size of the PEM systems is accompanied by a decrease in the spread of pore size distribution.

Regarding the transition to the "layer dominated" regime, again the theoretical model description matches very well with previous observations, here indicating pore closure at 6 BL and 9–10 BL for the PDADMAC/PSS and PAH/PAA system, respectively.

In addition to the pore size distribution, an effective thickness was fitted to the PEG retention and pure water permeability measurements. Here, the effective thickness is compared to thicknesses obtained in reflectometry measurements performed on silicon wafers [43,54] (see Fig. 8). After reaching the layer dominated regime a monotonous increase in effective layer thickness can be observed, which again fits nicely with the idea that a continuous thin film of PEM is built on top of the support membrane and is dominating transport. When comparing the effective thickness to the thickness measured via reflectometry a few things have to be considered.

Firstly, during the fabrication of PEMs typically two growth regimes can be observed [27,44,45]. In the initial layers at low total thickness, the incremental thickness per layer increases with film thickness. In this regime, the amount of available ionic sites of the previously incorporated polyelectrolyte and with that essentially the buffer capacity of the layer increases with layer thickness, resulting in a seemingly exponential layer growth (thermodynamic limit). After a certain PEM thickness, which is dependent on the PE system and coating conditions, the less mobile polyelectrolyte does not fully compensate for the ionic sites inside the multilayer in one coating step, resulting in a more linear increase in layer thickness with layer number (kinetic limit). This can also be seen in the reflectometry measurements of the two PEM systems. Here, again we assume that the layer growth in the "layer dominated" regime of the membranes is linear. Therefore the average incremental thickness of the last 4 BLs from reflectometry measurements is used as a reference.

Secondly, the measured film property in reflectometry concerns the adsorbed polyelectrolyte mass per area. This, however, does not account for the water incorporated in the multilayer and the resulting

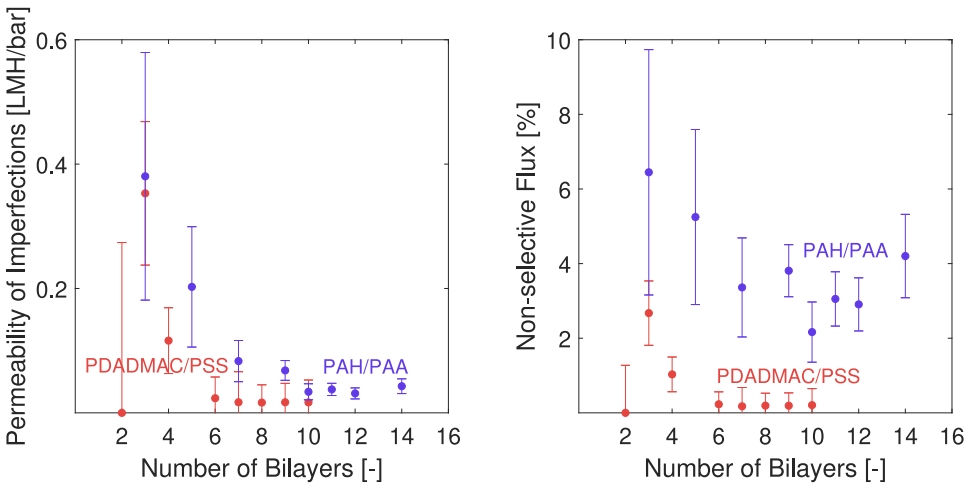

Fig. 9. Log-normal pore size distribution + imperfections fit. Absolute non-selective flux through imperfections by means of permeability [LMH/bar] (left) and relative non-selective permeate flux [%] (right) as a function of bilayer number [-]. Two Polyelectrolyte Multilayer systems: PDADMAC/PSS (red) and PAH/PAA (blue). Error bars display the 95% confidence intervals. (For interpretation of the references to color in this figure legend, the reader is referred to the web version of this article.)

change in layer thickness due to swelling. To transfer the measured mass density to a thickness, we assume a polyelectrolyte density of 1100 kgm^{-3} for both PEM systems [63]. In addition, to account for the thickness variation caused by swelling we assume a swelling degree of 35% for both systems [64–67]. Lastly, the effective membrane thickness fitted in the model already accounts for membrane porosity (< 1) and tortuosity (> 1), meaning that the actual layer thickness is lower than this value. Therefore, one expects the thickness obtained from reflectometry to be lower than the effective thickness obtained from the model fit.

When comparing the estimated thickness values from both methods, the thickness increment per BL obtained from reflectometry is about one order of magnitude lower for both PEM systems. In qualitative comparison, the thickness obtained for the different systems matches nicely in both characterization methods shown here. The PAH/PAA system forms thicker layers than the PDADMAC/PSS system (also clearly visible in the FESEM images shown in the Supporting Information S7).

4.5. Pore size distribution and imperfections

Another extension to the theoretical model concerns non-selective permeate flux (e.g. through imperfections in the PEM layer or module related leakage). In addition to improving the quality of the fit to the PEG retention data, one can obtain information on the pore closing behavior of the two PEM systems (where an open support pore with maximum retention of 6% towards PEG 3000 can be considered as non-selective) as well as the susceptibility of the PEM systems to imperfections. Lastly, considering the relative flux through imperfections one can estimate their influence on the observed retention.

Both the absolute amount of imperfections and the relative impact on the observed retention are displayed in Fig. 9 by means of the permeability through imperfections (to account for applied TMP) and the relative proportion of non-selective flux, respectively. The permeability of imperfections in the layer dominated regime is constantly low and very similar for both PEM systems (around 0.03 LMHbar). Thus, it is very likely the residual non-selective flux is caused by module related leakage and not by imperfections of the PEM system. From the amount of imperfections the transition from the "pore dominated" regime to the "layer dominated" regime can easily be spotted and fits very well with the previously determined 6 BL for PDADMAC/PSS and 9–10 BL for PAH/PAA.

To evaluate the impact of the non-selective flux on the observed retention one can simply look at the relative amount compared to the overall permeate flux. Due to the relatively high permeability of the PDADMAC/PSS system, the relative amount of non-selective flux is negligible and therefore not expected to affect the observed retention. The permeability of the PAH/PAA system, however, is one order of magnitude lower resulting in a more significant relative amount of non-selective flux (>3%). From the relative non-selective flux one can roughly estimate the maximally obtainable retention of the membrane module for a solute that is fully retained by the PEM layer using Eq. (28) (Ret < 97%). This outcome also explains why the PAH/PAA system, in contrast to the PDADMAC/PSS system and despite the smaller effective pore radius, does not reach full retention even for the 3000 Da PEG (see Fig. 5).

Lastly, one can consider the effect of constant intrinsic PEM properties with an increase of BL number in the "layer dominated" regime. With constant module related non-selective flux and continuously increasing hydraulic resistance, the relative proportion of non-selective flux will monotonously increase with increasing BL number. This trend is already indicated for the PAH/PAA system since the relative amount is already significant. As a result, the observed retention would continue to decrease with the BL number. The fitted pore size distributions are similar to the ones obtained without considering imperfections and are provided in the Supporting Information S8. Again, the mean pore radius in the "layer dominated" regime is 0.44 nm and 0.27 nm for the PDADMAC/PSS and the PAH/PAA system, respectively. However, there is a decrease in the spread of the pore size distribution σ for both systems from 98 pm to 96 pm and from 45 pm to 41 pm for PDADMAC/PSS and PAH/PAA, respectively.

4.6. Quality of fits

To quantify the benefit of using a pore size distribution to describe the PEM structure and predict PEG retention, we compare the quality of fits for the different theoretical model approaches by means of Mean Squared Error (MSE) (see Fig. 10). Graphs of fits using different model approaches for selected layer numbers can be found in the Supporting Information S9.

Here, again, it is very useful to distinguish the different regions of membrane structure for both PEM systems. Both PEM systems behave qualitatively very similar in the "pore dominated" regime. The introduction of a pore size distribution (which is quite broad in this regime) reduces the MSE by one order of magnitude. We attribute this to the influence of pore size distribution of the support membrane, which still influences the transport through the selective layer considerably.

The transition to the "layer dominated" regime is also visible in the quality of fit by a reduction in MSE by one order of magnitude.

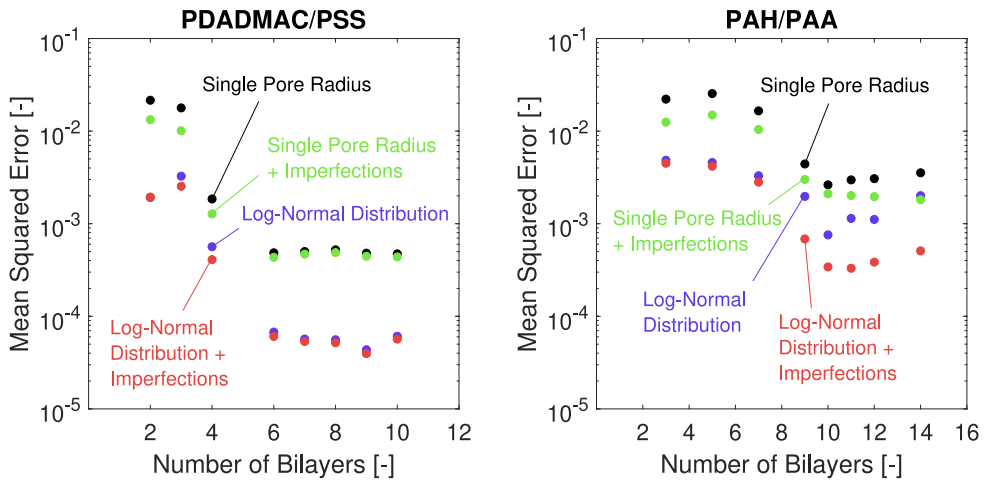

Fig. 10. Comparison of different pore size descriptions. Mean Squared Error [-] as a function of bilayer number [-]. Two Polyelectrolyte Multilayer systems: PDADMAC/PSS (left) and PAH/PAA (right).

This shows the difficulty to describe membrane transport in the "pore dominated" regime as a transition region between the bare support membrane and the PEM based thin film composite membrane. This transition region is characterized by a very heterogeneous membrane structure that is difficult to control and describe.

In the "layer dominated" regime both systems show a distinct difference in the quality of fit. The use of a log-normal pore size distribution while accounting for non-selective permeate flux reduces the MSE by one order of magnitude. However, a closer independent look at both structural effects reveals the dominating factors for both systems.

For the PDADMAC/PSS system, the pore size distribution is relatively broad and the relative impact of non-selective flux is almost negligible. Hence, accounting for imperfections only marginally reduces the MSE while accounting for the spread in pore size significantly reduces the MSE to (almost) the same value when accounting for both effects at the same time.

For the PAH/PAA system, the pore size distribution is relatively narrow and the relative impact of non-selective flux is considerable. Due to the narrow distribution in pore size, the fit quality does not improve as much compared to PDADMAC/PSS when adding a pore size distribution. The high relative impact of imperfections, however, results in a significant reduction of MSE when accounting for imperfections. When accounting for both effects at the same time, the MSE is again reduced by one order of magnitude compared to the single pore size model. A table with optimization parameters for the two selected systems, 10 BLs PDADMAC/PSS and 14 BLs PAH/PAA, for all models is shown in the Supporting Information S10.

It should be mentioned that the chosen correlation to define the size of PEG molecules depending on their molecular weight influences the effective structural representation of the PEMs to some extent. More details can be found in the Supporting Information S11.

4.7. Implications for the Polyelectrolyte Multilayer structure

When combining the results of the characterization techniques (both experimental and theoretical) applied in this study, we can deduce and compare the structural properties of the two PEM systems.

By fitting theoretical transport models with different effective structural PEM properties to PEG retention measurements, we can qualitatively compare the mesh size of the ionic crosslinking network of the PEM. Here, since we are interested in the intrinsic properties of the PEMs, it is important to consider membrane performance in the "layer dominated" regime. The higher retention of uncharged molecules, as well as, the higher hydraulic resistance of PAH/PAA over PDADMAC/PSS has also been observed in previous studies [32,68].

PDADMAC/PSS and PAH/PAA have a mean pore radius of 0.44 nm and 0.27 nm, respectively. Here, the order of magnitude matches well to the range of average pore size estimated based on uncharged solute transport in previous studies [39,69]. The difference between the two systems is in line with a previous study by Krasemann et al. [70], where it was shown that the charge density of the PEM system affects the mesh size of its ionic crosslinking network. The charge densities (defined for the repeating unit of the polyelectrolyte as the number of ion pairs/number of carbon atoms) of PDADMAC/PSS and PAH/PAA are 0.0625 and 0.167, respectively. Thus, the mesh size and with that the effective pore radius of PAH/PAA is expected to be smaller.

As the theoretical depiction of the PEM film (even when accounting for distribution in pore size) is still a simplification and the order of magnitude in pore size reaches the limit of continuum theory, one might wonder about the reliability and meaning of obtained effective pore radii. Therefore, we compared the obtained results on effective pore size distribution to results obtained by Chávez and Schönhoff [62], where an alternative approach was applied to determine pore size distributions in PEMs. Here, nuclear magnetic resonance cryoporometry was applied on PAH/PSS based PEMs coated on top of silica particles. Mean pore radii in the range of 0.6–0.75 nm were measured. Even though a different PEM system was studied the order of magnitude in pore size is comparable to the ones determined in this study. Therefore, we are convinced that indirectly determining pore radii via uncharged solute retention to the least gives a good estimate of the order of magnitude of PEM mesh size.

Another very relevant property regarding mesh size of PEMs is its dependency on BL number, as this will have crucial consequences on membrane design. In the study of Chávez and Schönhoff [62] the spread in pore size distribution did not vary with BL number, although the mean pore radius of the distribution slightly increased with BL number. This was attributed to the fact that, frequently, outer layers are less densely packed in PEMs. In our study, the effective pore size distribution in the "layer dominated" regime did not vary with BL number (within the range of uncertainties). These observations suggest there is an optimum BL number in membrane fabrication for uncharged solute retention, as after reaching the layer dominated regime additional BLs only increase the hydraulic resistance while not changing (or even increasing) the effective pore size.

In addition to pore radius, the fit of effective membrane thickness can give relevant information on the PEM systems. There are inherent limitations to directly comparing the effective thickness to the actual PEM thickness. One reason for this is that the effective thickness also includes tortuosity and porosity of the membrane. To unambiguously determine these three quantities, additional information is required.

Despite these inherent limitations, we have shown by the use of supplementary techniques (such as Reflectometry or FESEM) that the effective membrane thickness gives a very good qualitative indication of the PEM thickness.

When comparing the effective thickness increment per BL number in the "layer dominated" regime, a striking difference between the two PEM systems was observed. Here, PAH/PAA (689 nm/BL) has a more than ten times higher value in effective thickness than PDADMAC/PSS (44 nm/BL). Although one can certainly expect differences in tortuosity and porosity between those systems, this clearly indicates that PAH/PAA forms thicker layers under the selected coating conditions. This qualitative difference between the two PEM systems has been confirmed by additional measurement techniques.

The significantly different behavior in layer formation between PAH/PAA and PDADMAC/PSS under the chosen coating conditions is caused by the susceptibility of PE towards protonation. Both PAH (pKa 8–9 in solution [71]) and PAA (pKa 6.5 in solution [71]) are weak PEs, meaning their degree of charge is a function of pH. Both PDADMAC and PSS are strong PEs, meaning their degree of charge does not depend on pH in the used range. It has been shown that changes in the degree of charge in PEs can majorly influence the thickness of PEMs formed by those [71–76]. The group of Rubner has intensively studied the influence of pH (both during and after fabrication) on PEMs made of PAH/PAA [57,71,73,77]. It has been shown that the film thickness of PAH/PAA multilayers is very susceptible to solution pH during layer fabrication, where slight changes in pH can lead to a significant increase in layer thickness. In a pH range of 4.5 to 6, both layer thickness and surface roughness were substantially increased [73]. This was attributed to conformational changes of the PE chains to a more coiled one. This explains the very high film thicknesses observed in the present study, as the PEMs were coated at pH 5.5.

In contrast, the PEM build of PDADMAC and PSS (both PEs fully charged) forms significantly thinner layers. At the applied salt concentration (50 mM NaCl) the PEs are expected to adsorb in a flat configuration, resulting in compact layers [78].

Considering the just discussed intrinsic properties of both PEM systems, the observed closing behavior of the support pores seems rather contradictory. Even though PAH/PAA clearly forms much thicker PEM films, which in the declared "layer dominated" regime has a smaller effective pore size, the transition to the "layer dominated" regime is observed at higher BL numbers (9–10 BLs) than for PDADMAC/PSS (6 BLs).

Here, we want to propose a slightly adapted mechanism for closing the pores of the support membrane and forming a dense transport dominating separation layer. The hypothesis is, that these two processes do not necessarily happen simultaneously, but can be consecutive.

Although the PAH/PAA system fills the surface pores of the support membrane more quickly and forms thicker layers (explaining the much higher hydraulic resistance), the membrane properties, and with that, the intrinsic properties of the PEM, are still BL number dependent. Only after 9 BLs do the intrinsic properties of the PEM become independent of BL number. For the PDADMAC/PSS system, this clearly happens at a much lower layer thickness. Therefore, this transition does not depend on PEM thickness alone.

One potential explanation for the observed behavior could be an increasing density of the PAH/PAA layer with an increasing BL number (often the outermost layers of a PEM are less densely linked [23]). An indication of a distinct transition to a more dense selective layer is the increase in hydraulic resistance increment as a function of BL number after 9 BLs.

An alternative explanation could be that PAH/PAA multilayers coated in this pH regime are more prone to imperfections, which in addition have a higher impact on membrane performance. The relatively high amount of imperfections could be caused by a high surface roughness [73] and with that heterogeneity of the film as well as the relatively high rigidity of the PEM (with at the same time high mobilities of PEs inside the PEM [79]). To clearly identify the cause for the delayed transition to the "layer dominated" regime further studies are required.

5. Conclusion and outlook

In this work, we demonstrate the use of theoretical transport descriptions in combination with filtration measurements of uncharged molecules to be a simple but insightful technique to characterize PEM based NF membranes. The technique allows to properly predict membrane performance and provides indications on the intrinsic structure of PEMs. Thus, it can be used to systematically study the influence of coating conditions on PEM properties.

The two PEM systems studied in this work, PDADMAC/PSS and PAH/PAA, showed very distinctive differences in structural properties. Both systems were represented by a relatively narrow distribution in pore radius in the order of 0.3–0.5 nm. However, the spread in pore radius represented by a log-normal distribution of PAH/PAA (0.04 nm) is smaller than of PDADMAC/PSS (0.1 nm). Accordingly, PAH/PAA clearly formed denser (0.27 nm) and thicker (689 nm/BL) films in comparison to PDADMAC/PSS (0.44 nm, 44 nm/BL). These differences match very well with the previous studies on these PEM systems by other groups as well as with our FESEM measurements.

Another useful feature of this technique is, that it reveals the transition of a support dominated membrane (UF) to a PEM layer dominated membrane (NF) with an increasing number of coating layers. Here, unexpectedly the PDADMAC/PSS system transitions at a smaller number of bilayers. This could indicate a fundamentally different mechanism of separation layer formation for both PEM systems. However, more studies are required to identify the exact mechanisms.

It was also shown, that (within the range of BL numbers studied) the intrinsic network structure of the PEMs is independent of the BL number. This has important implications for the fabrication of NF membranes. With an increasing layer thickness at a constant effective pore size, the energy efficiency of the membrane decreases. Thus, we propose there is an optimum separation layer thickness for the retention of uncharged molecules.

Finally, the observations of this study again underline the potential of PEMs as selective layers for NF membranes. Compared to the dominantly applied polyamide-based thin film composite membranes, similar ranges in pore size can be obtained with superior control of film thickness and structure. Especially promising is the use of asymmetric PEM films for NF applications, to avoid the considerable penalty in hydraulic resistance that is inherent for dense PEM systems during the closure of the underlying support pores to form a selective layer.

CRediT authorship contribution statement

Moritz A. Junker: Methodology, Conceptualization, Investigation, Formal analysis, Writing – original draft. **Wiebe M. de Vos:** Funding acquisition, Supervision, Conceptualization, Writing – review & editing. **Joris de Grooth:** Funding acquisition, Supervision, Conceptualization, Writing – review & editing. **Rob G.H. Lammertink:** Funding acquisition, Supervision, Conceptualization, Writing – review & editing.

Declaration of competing interest

The authors declare the following financial interests/personal relationships which may be considered as potential competing interests: Dr. J de Grooth currently holds a part-time position at NX Filtration B.V., a membrane manufacturer. The other authors declare that they have no known competing financial interests or personal relationships that could have appeared to influence the work reported in this paper.

Data availability

Data will be made available via 4TU.data after acceptance/publication.

Acknowledgments

This project was made possible through financial support of Oasen (Gouda, Netherlands), NX Filtration (Enschede, Netherlands), and the TKI HTSM, through the University of Twente connecting industry program. The authors would like to thank Jeffery A. Wood for his useful advice and discussions.

Appendix A. Supplementary data

Supplementary material related to this article can be found online at https://doi.org/10.1016/j.memsci.2022.121164. It contains details on experimental methods and modelling procedures, as well as, FESEM images of the membranes.

References

[1] D.L. Oatley-Radcliffe, M. Walters, T.J. Ainscough, P.M. Williams, A.W. Mohammad, N. Hilal, Nanofiltration membranes and processes: A review of research trends over the past decade, J. Water Process Eng. 19 (2017) 164–171, http://dx.doi.org/10.1016/j.jwpe.2017.07.026.

[2] A.W. Mohammad, Y.H. Teow, W.L. Ang, Y.T. Chung, D.L. Oatley-Radcliffe, N. Hilal, Nanofiltration membranes review: Recent advances and future prospects, Desalination 356 (2015) 226–254, http://dx.doi.org/10.1016/j.desal.2014.10.043.

[3] B. Van der Bruggen, C. Vandecasteele, Removal of pollutants from surface water and groundwater by nanofiltration: overview of possible applications in the drinking water industry, Environ. Pollut. 122 (3) (2003) 435–445, http://dx.doi.org/10.1016/S0269-7491(02)00308-1.

[4] K. Nath, H.K. Dave, T.M. Patel, Revisiting the recent applications of nanofiltration in food processing industries: Progress and prognosis, Trends Food Sci. Technol. 73 (2018) 12–24, http://dx.doi.org/10.1016/j.tifs.2018.01.001.

[5] C. de Morais Coutinho, M.C. Chiu, R.C. Basso, A.P.B. Ribeiro, L.A.G. Gonçalves, L.A. Viotto, State of art of the application of membrane technology to vegetable oils: A review, Food Res. Int. 42 (5) (2009) 536–550, http://dx.doi.org/10.1016/j.foodres.2009.02.010.

[6] M.G. Buonomenna, J. Bae, Organic solvent nanofiltration in pharmaceutical industry, Sep. Purif. Rev. 44 (2) (2015) 157–182, http://dx.doi.org/10.1080/15422119.2014.918884.

[7] W.-J. Lau, A.F. Ismail, Polymeric nanofiltration membranes for textile dye wastewater treatment: Preparation, performance evaluation, transport modelling, and fouling control — a review, Desalination 245 (1) (2009) 321–348, http://dx.doi.org/10.1016/j.desal.2007.12.058.

[8] M. Beeftink, B. Hofs, O. Kramer, I. Odegard, A. van der Wal, Carbon footprint of drinking water softening as determined by life cycle assessment, J. Cleaner Prod. 278 (2021) 123925, http://dx.doi.org/10.1016/j.jclepro.2020.123925.

[9] S. Kim, K.H. Chu, Y.A.J. Al-Hamadani, C.M. Park, M. Jang, D.-H. Kim, M. Yu, J. Heo, Y. Yoon, Removal of contaminants of emerging concern by membranes in water and wastewater: A review, Chem. Eng. J. 335 (2018) 896–914, http://dx.doi.org/10.1016/j.cej.2017.11.044.

[10] B. Van der Bruggen, M. Mänttäri, M. Nyström, Drawbacks of applying nanofiltration and how to avoid them: A review, Sep. Purif. Technol. 63 (2) (2008) 251–263, http://dx.doi.org/10.1016/j.seppur.2008.05.010.

[11] H. Zhang, Q. He, J. Luo, Y. Wan, S.B. Darling, Sharpening nanofiltration: Strategies for enhanced membrane selectivity, ACS Appl. Mater. Interfaces 12 (36) (2020) 39948–39966, http://dx.doi.org/10.1021/acsami.0c11136.

[12] R. Zhang, J. Tian, S. Gao, B. Van der Bruggen, How to coordinate the trade-off between water permeability and salt rejection in nanofiltration? J. Mater. Chem. A 8 (18) (2020) 8831–8847, http://dx.doi.org/10.1039/D0TA02510K.

[13] M.Q. Seah, W.J. Lau, P.S. Goh, H.-H. Tseng, R.A. Wahab, A.F. Ismail, Progress of interfacial polymerization techniques for polyamide thin film (nano)composite membrane fabrication: A comprehensive review, Polymers 12 (12) (2020) 2817, http://dx.doi.org/10.3390/polym12122817.

[14] Z. Yang, Y. Zhou, Z. Feng, X. Rui, T. Zhang, Z. Zhang, A review on reverse osmosis and nanofiltration membranes for water purification, Polymers 11 (8) (2019) 1252, http://dx.doi.org/10.3390/polym11081252.

[15] R.J. Petersen, Composite reverse osmosis and nanofiltration membranes, J. Membr. Sci. 83 (1) (1993) 81–150, http://dx.doi.org/10.1016/0376-7388(93)80014-O.

[16] V.T. Do, C.Y. Tang, M. Reinhard, J.O. Leckie, Effects of chlorine exposure conditions on physiochemical properties and performance of a polyamide membrane—Mechanisms and implications, Environ. Sci. Technol. 46 (24) (2012) 13184–13192, http://dx.doi.org/10.1021/es302867f.

[17] W. Jin, A. Toutianoush, B. Tieke, Use of polyelectrolyte layer-by-layer assemblies as nanofiltration and reverse osmosis membranes, Langmuir 19 (7) (2003) 2550–2553, http://dx.doi.org/10.1021/la020926f.

[18] B.W. Stanton, J.J. Harris, M.D. Miller, M.L. Bruening, Ultrathin, multilayered polyelectrolyte films as nanofiltration membranes, Langmuir 19 (17) (2003) 7038–7042, http://dx.doi.org/10.1021/la034603a.

[19] N. Joseph, P. Ahmadiannamini, R. Hoogenboom, I.F.J. Vankelecom, Layer-by-layer preparation of polyelectrolyte multilayer membranes for separation, Polym. Chem. 5 (6) (2014) 1817–1831, http://dx.doi.org/10.1039/c3py01262j.

[20] X. Li, C. Liu, B. Van der Bruggen, Polyelectrolytes self-assembly: versatile membrane fabrication strategy, J. Mater. Chem. A 8 (40) (2020) 20870–20896, http://dx.doi.org/10.1039/D0TA07154D.

[21] E. te Brinke, I. Achterhuis, D.M. Reurink, J. de Grooth, W.M. de Vos, Multiple approaches to the buildup of asymmetric polyelectrolyte multilayer membranes for efficient water purification, ACS Appl. Polym. Mater. 2 (2) (2020) 715–724, http://dx.doi.org/10.1021/acsapm.9b01038.

[22] E.N. Durmaz, S. Sahin, E. Virga, S. de Beer, L.C.P.M. de Smet, W.M. de Vos, Polyelectrolytes as building blocks for next-generation membranes with advanced functionalities, ACS Appl. Polym. Mater. 3 (9) (2021) 4347–4374, http://dx.doi.org/10.1021/acsapm.1c00654.

[23] R. v. Klitzing, Internal structure of polyelectrolyte multilayer assemblies, Phys. Chem. Chem. Phys. 8 (43) (2006) 5012–5033, http://dx.doi.org/10.1039/B607760A.

[24] M. Schönhoff, V. Ball, A.R. Bausch, C. Dejugnat, N. Delorme, K. Glinel, R.v. Klitzing, R. Steitz, Hydration and internal properties of polyelectrolyte multilayers, Colloids Surf., A 303 (1) (2007) 14–29, http://dx.doi.org/10.1016/j.colsurfa.2007.02.054.

[25] D.M. Reurink, J.P. Haven, I. Achterhuis, S. Lindhoud, H.D.W. Roesink, W.M. de Vos, Annealing of polyelectrolyte multilayers for control over ion permeation, Adv. Mater. Interfaces 5 (20) (2018) 1800651, http://dx.doi.org/10.1002/admi.201800651.

[26] I.J. Gresham, D.M. Reurink, S.W. Prescott, A.R.J. Nelson, W.M. de Vos, J.D. Willott, Structure and hydration of asymmetric polyelectrolyte multilayers as studied by neutron reflectometry: Connecting multilayer structure to superior membrane performance, Macromolecules 53 (23) (2020) 10644–10654, http://dx.doi.org/10.1021/acs.macromol.0c01909.

[27] H.M. Fares, J.B. Schlenoff, Diffusion of sites versus polymers in polyelectrolyte complexes and multilayers, J. Am. Chem. Soc. 139 (41) (2017) 14656–14667, http://dx.doi.org/10.1021/jacs.7b07905.

[28] W.R. Bowen, J.S. Welfoot, Modelling of membrane nanofiltration—pore size distribution effects, Chem. Eng. Sci. 57 (8) (2002) 1393–1407, http://dx.doi.org/10.1016/s0009-2509(01)00412-2.

[29] K. Košutić, L. Kaštelan-Kunst, B. Kunst, Porosity of some commercial reverse osmosis and nanofiltration polyamide thin-film composite membranes, J. Membr. Sci. 168 (1) (2000) 101–108, http://dx.doi.org/10.1016/S0376-7388(99)00309-9.

[30] J.A. Otero, O. Mazarrasa, J. Villasante, V. Silva, P. Prádanos, J.I. Calvo, A. Hernández, Three independent ways to obtain information on pore size distributions of nanofiltration membranes, J. Membr. Sci. 309 (1) (2008) 17–27, http://dx.doi.org/10.1016/j.memsci.2007.09.065.

[31] R.R. Sharma, R. Agrawal, S. Chellam, Temperature effects on sieving characteristics of thin-film composite nanofiltration membranes: pore size distributions and transport parameters, J. Membr. Sci. 223 (1) (2003) 69–87, http://dx.doi.org/10.1016/S0376-7388(03)00310-7.

[32] M.G. Elshof, W.M. de Vos, J. de Grooth, N.E. Benes, On the long-term pH stability of polyelectrolyte multilayer nanofiltration membranes, J. Membr. Sci. 615 (2020) 118532, http://dx.doi.org/10.1016/j.memsci.2020.118532.

[33] M.A. Junker, W.M. de Vos, R.G.H. Lammertink, J. de Grooth, Bridging the gap between lab-scale and commercial dimensions of hollow fiber nanofiltration membranes, J. Membr. Sci. 624 (2021) 119100, http://dx.doi.org/10.1016/j.memsci.2021.119100.

[34] J. Newman, Extension of the Lévêque solution, Lawrence Berkeley Natl. Lab., [Rep.] LBNL, 1967.

[35] V. Geraldes, M.D. Afonso, Generalized mass-transfer correction factor for nanofiltration and reverse osmosis, AIChE J. 52 (10) (2006) 3353–3362, http://dx.doi.org/10.1002/aic.10968.

[36] M. Tomšič, M. Bešter-Rogač, A. Jamnik, R. Neueder, J. Barthel, Conductivity of magnesium sulfate in water from 5 to 35° C and from infinite dilution to saturation, J. Solution Chem. 31 (1) (2002) 19–31, http://dx.doi.org/10.1023/A:1014853001357.

[37] W.R. Bowen, A.W. Mohammad, N. Hilal, Characterisation of nanofiltration membranes for predictive purposes — use of salts, uncharged solutes and atomic force microscopy, J. Membr. Sci. 126 (1) (1997) 91–105, http://dx.doi.org/10.1016/S0376-7388(96)00276-1.

[38] S. Bandini, D. Vezzani, Nanofiltration modeling: the role of dielectric exclusion in membrane characterization, Chem. Eng. Sci. 58 (15) (2003) 3303–3326, http://dx.doi.org/10.1016/s0009-2509(03)00212-4.

[39] X. Liu, M.L. Bruening, Size-selective transport of uncharged solutes through multilayer polyelectrolyte membranes, Chem. Mater. 16 (2) (2004) 351–357, http://dx.doi.org/10.1021/cm034559k.

[40] A. Szymczyk, M. Sbaï, P. Fievet, A. Vidonne, Transport properties and electrokinetic characterization of an amphoteric nanofilter, Langmuir 22 (8) (2006) 3910–3919, http://dx.doi.org/10.1021/la051888d.

[41] R.B. Bird, W.E. Stewart, E.N. Lightfoot, Transport Phenomena, second ed., John Wiley & Sons, Inc., New York, 2002, p. 529.
[42] V. Murugaiah, R.E. Synovec, Radial measurement of hydrodynamically generated concentration profiles for molecular weight determination, Anal. Chem. 64 (18) (1992) 2130–2137, http://dx.doi.org/10.1021/ac00042a018.
[43] J.d. Grooth, R. Oborný, J. Potreck, K. Nijmeijer, W.M.d. Vos, The role of ionic strength and odd–even effects on the properties of polyelectrolyte multilayer nanofiltration membranes, J. Membr. Sci. 475 (2015) 311–319, http://dx.doi.org/10.1016/j.memsci.2014.10.044.
[44] R.A. Ghostine, M.Z. Markarian, J.B. Schlenoff, Asymmetric growth in polyelectrolyte multilayers, J. Am. Chem. Soc. 135 (20) (2013) 7636–7646, http://dx.doi.org/10.1021/ja401318m.
[45] K.D. Kelly, H.M. Fares, S. Abou Shaheen, J.B. Schlenoff, Intrinsic properties of polyelectrolyte multilayer membranes: Erasing the memory of the interface, Langmuir 34 (13) (2018) 3874–3883, http://dx.doi.org/10.1021/acs.langmuir.8b00336.
[46] S.B. Abbott, W.M. de Vos, L.L.E. Mears, R. Barker, R.M. Richardson, S.W. Prescott, Hydration of odd–even terminated polyelectrolyte multilayers under mechanical confinement, Macromolecules 47 (10) (2014) 3263–3273, http://dx.doi.org/10.1021/ma500557m.
[47] S. Hong, M. Elimelech, Chemical and physical aspects of natural organic matter (NOM) fouling of nanofiltration membranes, J. Membr. Sci. 132 (2) (1997) 159–181, http://dx.doi.org/10.1016/S0376-7388(97)00060-4.
[48] C. Ba, D.A. Ladner, J. Economy, Using polyelectrolyte coatings to improve fouling resistance of a positively charged nanofiltration membrane, J. Membr. Sci. 347 (1) (2010) 250–259, http://dx.doi.org/10.1016/j.memsci.2009.10.031.
[49] W. Yu, T. Liu, J. Crawshaw, T. Liu, N. Graham, Ultrafiltration and nanofiltration membrane fouling by natural organic matter: Mechanisms and mitigation by pre-ozonation and pH, Water Res. 139 (2018) 353–362, http://dx.doi.org/10.1016/j.watres.2018.04.025.
[50] M. Mänttäri, L. Puro, J. Nuortila-Jokinen, M. Nyström, Fouling effects of polysaccharides and humic acid in nanofiltration, J. Membr. Sci. 165 (1) (2000) 1–17, http://dx.doi.org/10.1016/S0376-7388(99)00215-X.
[51] H. Song, J. Shao, Y. He, J. Hou, W. Chao, Natural organic matter removal and flux decline with charged ultrafiltration and nanofiltration membranes, J. Membr. Sci. 376 (1) (2011) 179–187, http://dx.doi.org/10.1016/j.memsci.2011.04.022.
[52] J.G. Wijmans, R.W. Baker, The solution-diffusion model: a review, J. Membr. Sci. 107 (1–2) (1995) 1–21, http://dx.doi.org/10.1016/0376-7388(95)00102-i.
[53] N. Kavokine, R.R. Netz, L. Bocquet, Fluids at the nanoscale: From continuum to subcontinuum transport, Annu. Rev. Fluid Mech. 53 (1) (2021) 377–410, http://dx.doi.org/10.1146/annurev-fluid-071320-095958.
[54] J.A. Regenspurg, A.F. Martins Costa, I. Achterhuis, W.M. de Vos, Influence of molecular weight on the performance of polyelectrolyte multilayer nanofiltration membranes, ACS Appl. Polym. Mater. 4 (5) (2022) 2962–2971, http://dx.doi.org/10.1021/acsapm.1c00826.
[55] N. Hilal, H. Al-Zoubi, N.A. Darwish, A.W. Mohammad, Characterisation of nanofiltration membranes using atomic force microscopy, Desalination 177 (1) (2005) 187–199, http://dx.doi.org/10.1016/j.desal.2004.12.008.
[56] A.W. Mohammad, N. Ali, N. Hilal, Investigating characteristics of increasing molecular weight cutoff polyamide nanofiltration membranes using solutes rejection and atomic force microscopy, Sep. Sci. Technol. 38 (6) (2003) 1307–1327, http://dx.doi.org/10.1081/SS-120018811.
[57] D. Yoo, S.S. Shiratori, M.F. Rubner, Controlling bilayer composition and surface wettability of sequentially adsorbed multilayers of weak polyelectrolytes, Macromolecules 31 (13) (1998) 4309–4318, http://dx.doi.org/10.1021/ma9800360.
[58] D. Laurent, J.B. Schlenoff, Multilayer assemblies of redox polyelectrolytes, Langmuir 13 (6) (1997) 1552–1557, http://dx.doi.org/10.1021/la960959t.
[59] J.B. Schlenoff, H. Ly, M. Li, Charge and mass balance in polyelectrolyte multilayers, J. Am. Chem. Soc. 120 (30) (1998) 7626–7634, http://dx.doi.org/10.1021/ja980350+.
[60] G. Decher, Fuzzy nanoassemblies: Toward layered polymeric multicomposites, Science 277 (5330) (1997) 1232–1237, http://dx.doi.org/10.1126/science.277.5330.1232.
[61] M. Lösche, J. Schmitt, G. Decher, W.G. Bouwman, K. Kjaer, Detailed structure of molecularly thin polyelectrolyte multilayer films on solid substrates as revealed by neutron reflectometry, Macromolecules 31 (25) (1998) 8893–8906, http://dx.doi.org/10.1021/ma980910p.
[62] F.V. Chávez, M. Schönhoff, Pore size distributions in polyelectrolyte multilayers determined by nuclear magnetic resonance cryoporometry, J. Chem. Phys. 126 (10) (2007) 104705, http://dx.doi.org/10.1063/1.2565841.
[63] R. Köhler, I. Dönch, P. Ott, A. Laschewsky, A. Fery, R. Krastev, Neutron reflectometry study of swelling of polyelectrolyte multilayers in water vapors: Influence of charge density of the polycation, Langmuir 25 (19) (2009) 11576–11585, http://dx.doi.org/10.1021/la901508w.
[64] S. Dodoo, B.N. Balzer, T. Hugel, A. Laschewsky, R.v. Klitzing, Effect of ionic strength and layer number on swelling of polyelectrolyte multilayers in water vapour, Soft Mater. 11 (2) (2013) 157–164, http://dx.doi.org/10.1080/1539445X.2011.607203.
[65] E. Guzmán, H. Ritacco, J.E.F. Rubio, R.G. Rubio, F. Ortega, Salt-induced changes in the growth of polyelectrolyte layers of poly(diallyl-dimethylammonium chloride) and poly(4-styrene sulfonate of sodium), Soft Matter 5 (10) (2009) 2130–2142, http://dx.doi.org/10.1039/B901193E.
[66] O.M. Tanchak, C.J. Barrett, Swelling dynamics of multilayer films of weak polyelectrolytes, Chem. Mater. 16 (14) (2004) 2734–2739, http://dx.doi.org/10.1021/cm049920x.
[67] A. Vidyasagar, C. Sung, K. Losensky, J.L. Lutkenhaus, pH-dependent thermal transitions in hydrated layer-by-layer assemblies containing weak polyelectrolytes, Macromolecules 45 (22) (2012) 9169–9176, http://dx.doi.org/10.1021/ma3020454.
[68] S.U. Hong, R. Malaisamy, M.L. Bruening, Optimization of flux and selectivity in Cl/SO42-separations with multilayer polyelectrolyte membranes, J. Membr. Sci. 283 (1) (2006) 366–372, http://dx.doi.org/10.1016/j.memsci.2006.07.007.
[69] W. Jin, A. Toutianoush, B. Tieke, Size- and charge-selective transport of aromatic compounds across polyelectrolyte multilayer membranes, Appl. Surf. Sci. 246 (4) (2005) 444–450, http://dx.doi.org/10.1016/j.apsusc.2004.11.067.
[70] L. Krasemann, A. Toutianoush, B. Tieke, Self-assembled polyelectrolyte multilayer membranes with highly improved pervaporation separation of ethanol/water mixtures, J. Membr. Sci. 181 (2) (2001) 221–228, http://dx.doi.org/10.1016/S0376-7388(00)00535-4.
[71] J. Choi, M.F. Rubner, Influence of the degree of ionization on weak polyelectrolyte multilayer assembly, Macromolecules 38 (1) (2005) 116–124, http://dx.doi.org/10.1021/ma048596o.
[72] M. Elzbieciak, M. Kolasinska, P. Warszynski, Characteristics of polyelectrolyte multilayers: The effect of polyion charge on thickness and wetting properties, Colloids Surf., A 321 (1) (2008) 258–261, http://dx.doi.org/10.1016/j.colsurfa.2008.01.036.
[73] S. Shiratori, M. Rubner, pH-dependent thickness behavior of sequentially adsorbed layers of weak polyelectrolytes, Macromolecules 33 (2000) http://dx.doi.org/10.1021/ma991645q.
[74] U. Voigt, W. Jaeger, G.H. Findenegg, R.v. Klitzing, Charge effects on the formation of multilayers containing strong polyelectrolytes, J. Phys. Chem. B 107 (22) (2003) 5273–5280, http://dx.doi.org/10.1021/jp0256488.
[75] R. Steitz, W. Jaeger, R.v. Klitzing, Influence of charge density and ionic strength on the multilayer formation of strong polyelectrolytes, Langmuir 17 (15) (2001) 4471–4474, http://dx.doi.org/10.1021/la010168d.
[76] K. Glinel, A. Moussa, A.M. Jonas, A. Laschewsky, Influence of polyelectrolyte charge density on the formation of multilayers of strong polyelectrolytes at low ionic strength, Langmuir 18 (4) (2002) 1408–1412, http://dx.doi.org/10.1021/la0113670.
[77] J.D. Mendelsohn, C.J. Barrett, V.V. Chan, A.J. Pal, A.M. Mayes, M.F. Rubner, Fabrication of microporous thin films from polyelectrolyte multilayers, Langmuir 16 (11) (2000) 5017–5023, http://dx.doi.org/10.1021/la000075g.
[78] X. Zan, D.A. Hoagland, T. Wang, Z. Su, Ion dispositions in polyelectrolyte multilayer films, Macromolecules 45 (21) (2012) 8805–8812, http://dx.doi.org/10.1021/ma3014492.
[79] P. Bieker, M. Schönhoff, Linear and exponential growth regimes of multilayers of weak polyelectrolytes in dependence on pH, Macromolecules 43 (11) (2010) 5052–5059, http://dx.doi.org/10.1021/ma1007489.